

# Proximity-dependent Mapping of the Androgen Receptor Identifies Krüppel-like Factor 4 as a Functional Partner

## Authors

Lauriane Vélot, Frédéric Lessard, Félix-Antoine Bérubé-Simard, Christophe Tav, Bertrand Neveu, Valentine Teyssier, Imène Boudaoud, Ugo Dionne, Noémie Lavoie, Steve Bilodeau, Frédéric Pouliot, and Nicolas Bisson

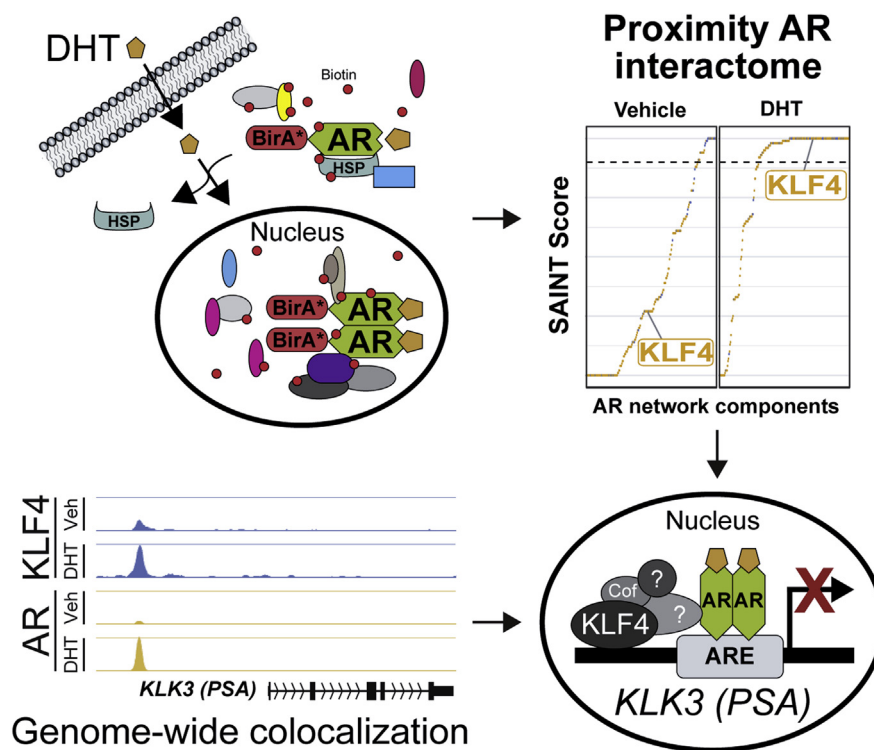
## Correspondence

frederic.pouliot@  
crchudequebec.ulaval.ca; nick.  
bisson@crchudequebec.ulaval.  
ca

## In Brief

A proximity interaction network for the androgen receptor (AR) was obtained from androgen-responsive prostate cancer cells. A total of 267 candidates were identified, most associating following ligand stimulation, including Krüppel-like factor 4 (KLF4). KLF4 and AR were found to colocalize genome-wide on 4097 genes including *PSA* (*KLK3*), for which KLF4 acts as a repressor, without regulating the expression of AR. These results are instrumental to further dissect the molecular mechanisms underlying androgen signaling in prostate cells.

## Graphical Abstract



## Highlights

- BiID proteomics identifies 267 androgen receptor (AR)-associated candidates
- Krüppel-like factor 4 (KLF4) is a new AR interaction partner
- AR and KLF4 colocalize genome-wide on >4000 genes, including *KLK3* (*PSA*)
- KLF4 acts as a repressor for the AR target gene *KLK3* (*PSA*)

# Proximity-dependent Mapping of the Androgen Receptor Identifies Kruppel-like Factor 4 as a Functional Partner

Lauriane Vélot<sup>1,2,3</sup>, Frédéric Lessard<sup>1,2,3</sup>, Félix-Antoine Bérubé-Simard<sup>1,2</sup>,  
Christophe Tav<sup>1,2,4</sup>, Bertrand Neveu<sup>1,2</sup>, Valentine Teyssier<sup>1,2,3</sup>, Imène Boudaoud<sup>1,2</sup>,  
Ugo Dionne<sup>1,2,3</sup>, Noémie Lavoie<sup>1,2,3</sup>, Steve Bilodeau<sup>1,2,4,5</sup>, Frédéric Pouliot<sup>1,2,6,\*</sup>, and  
Nicolas Bisson<sup>1,2,3,5,\*</sup> 

Prostate cancer (PCa) is the most frequently diagnosed cancer in men and the third cause of cancer mortality. PCa initiation and growth are driven by the androgen receptor (AR). The AR is activated by androgens such as testosterone and controls prostatic cell proliferation and survival. Here, we report an AR signaling network generated using BiLD proximity labeling proteomics in androgen-dependent LAPC4 cells. We identified 31 AR-associated proteins in nonstimulated cells. Strikingly, the AR signaling network increased to 182 and 200 proteins, upon 24 h or 72 h of androgenic stimulation, respectively, for a total of 267 nonredundant AR-associated candidates. Among the latter group, we identified 213 proteins that were not previously reported in databases. Many of these new AR-associated proteins are involved in DNA metabolism, RNA processing, and RNA polymerase II transcription. Moreover, we identified 44 transcription factors, including the Krüppel-like factor 4 (KLF4), which were found interacting in androgen-stimulated cells. Interestingly, KLF4 repressed the well-characterized AR-dependent transcription of the *KLK3* (PSA) gene; AR and KLF4 also colocalized genome-wide. Taken together, our data report an expanded high-confidence proximity network for AR, which will be instrumental to further dissect the molecular mechanisms underlying androgen signaling in PCa cells.

Prostate cancer (PCa) is the most frequently diagnosed cancer in men and is the third cause of cancer mortality (1). PCa initiation and growth are driven by the androgen receptor (NR3C4, AR), a steroid receptor that belongs to the nuclear receptor family (2). Following binding by androgens such as dihydrotestosterone (DHT) in the cytoplasm, AR undergoes a conformational change, which allows its release from heat

shock chaperone proteins (HSPs) and the formation of phosphorylated AR homodimers (3, 4). AR is then able to translocate to the nucleus where it binds DNA on androgen response elements (AREs). As a transcription factor (TF), AR regulates along with cofactors the transcription of target genes involved in proliferation, survival, and cell growth or acts as a cofactor for other TFs (5, 6). Its best characterized target gene is *Kallikrein-Related Peptidase 3* (*KLK3*), often referred to as *Prostate-Specific Antigen* (PSA). Moreover, AR is phosphorylated and activated in a ligand-independent manner by kinases such as MAPK and PI3K/AKT (7, 8). Thus, AR function is regulated by a number of proteins that affect ligand binding, protein folding, nuclear translocation, and transcriptional activation. However, the extent of these AR-associated proteins is still poorly understood.

Several studies shed light on AR protein interaction networks using unbiased approaches such as affinity purification combined to mass spectrometry (AP-MS). Using matrix-assisted laser desorption ionization time-of-flight (MALDI-TOF) MS on purified AR complexes, Ishitani *et al.* identified a number of associated proteins including RNA-binding protein P54NRB/NONO (9). They further demonstrated that it functions as a transcriptional coactivator for AR. In another report, Faus *et al.* utilized DNA corresponding to ARE-2 as bait to characterize AR complexes using MS and identified the ubiquitin-specific protease USP10 (10). Mayeur *et al.* performed pull-downs using GST-tagged AR N-terminal or C-terminal polypeptides combined to MS to delineate an association between AR and the DNA-dependent protein kinase (DNA-PK) complex (11). Likewise, Chen *et al.* utilized AR AP-MS to discover an androgen-dependent association

From the <sup>1</sup>Centre de recherche du Centre Hospitalier Universitaire (CHU) de Québec-Université Laval, Axe Oncologie, Québec, Quebec, Canada; <sup>2</sup>Centre de recherche sur le cancer de l'Université Laval, Québec, Quebec, Canada; <sup>3</sup>PROTEO-Quebec Network for Research on Protein Function, Engineering, and Applications, Québec, Quebec, Canada; <sup>4</sup>Centre de recherche en données massives de l'Université Laval, Québec, Québec, Canada; <sup>5</sup>Department of Molecular Biology, Medical Biochemistry and Pathology, Faculté de Médecine, and <sup>6</sup>Department of Surgery, Faculté de Médecine, Université Laval, Québec, Quebec, Canada

\*For correspondence: Frédéric Pouliot, [frederic.pouliot@crchudequebec.ulaval.ca](mailto:frederic.pouliot@crchudequebec.ulaval.ca); Nicolas Bisson, [nick.bisson@crchudequebec.ulaval.ca](mailto:nick.bisson@crchudequebec.ulaval.ca).

between endogenous AR and the deubiquitinating enzyme USP7 (12). More recently, a few groups reported the identification of AR-associated proteins at a larger scale. Paltoglou *et al.* took advantage of the RIME method (rapid immunoprecipitation MS of endogenous proteins) to identify 54 and 75 candidates with wild-type AR and the constitutively active ARv567es variant, respectively. Interestingly, they identified the transcription factor Grainyhead-like 2 (GRHL2) and characterized its function as a coregulator of AR, both as an oncogenic enhancer of androgen signaling and as a suppressor of metastasis (13). In another study, Stelloo *et al.* also made use of RIME and reported 66 proteins in the AR interaction network in LNCaP cells. They further validated some of these interactions in LAPC4 cells and in prostate cancer patient-derived xenograft models (14). Hsiao *et al.* took advantage of cellular fractionation to determine the cytosolic AR protein interactome and to identify proteins implicated in androgen-dependent AR-mediated gene transcription (15, 16). Paliouras *et al.* used three AR genetic variants and delineated their protein interaction network to help predict prostate cancer clinical outcome (17). While these AP-based MS approaches have been instrumental for the characterization of AR protein interaction networks, they have often come short of identifying proteins displaying weaker or more transient interactions due to technical limitations (18).

To circumvent this, Roux *et al.* developed proximity labeling proteomics, namely BioID (19), a method based on the fusion of a mutant biotin ligase BirA\* with a protein of interest. Upon addition of biotin to the culture medium, the promiscuous BirA\* chimera will favor covalent biotin binding to adjacent proteins, which may be affinity-purified and identified by MS. Lempiainen *et al.* used this approach to define a proximity network for either glucocorticoid receptor and AR overexpressed in DHT-stimulated human embryonic kidney (HEK) 293 cells (20), which do not endogenously express detectable levels of AR (21). A total of 32 DHT-dependent high-confidence proximity interactions were identified. Among this group, ten were previously reported in the BioGRID, GPS-

Prot, or IntAct databases (22–24), including NCOR1 (25), JMJD1C (26), SMARCA4/BRG1 and SMARCD1/BAF60a (27), and TCF20/SPBP (28).

Here, we performed BioID proximity labeling proteomics in androgen-dependent LAPC4 cells that express wild-type AR. We delineate an AR proximity network containing 267 proteins, most of which associated following ligand stimulation, providing a large high-confidence interaction network for AR obtained from androgen-responsive cells. Among the AR-associated proteins, we reveal 213 candidates that were not previously reported in the BioGRID, GSP-Prot, or IntAct database and describe the identification of the Krüppel-like factor 4 (KLF4) as a new AR-associated protein. Finally, we show that KLF4 and AR colocalize genome-wide on a number of genes including PSA (*KLK3*) and surprisingly act as a repressor for the latter, without regulating the expression of AR itself.

EXPERIMENTAL PROCEDURES

Plasmid Constructions and Adenoviral Production

Human AR (NCBI clone NP\_000035.2) was subcloned into pMSCVpuro (Clontech) in fusion with an N-terminal 3xFLAG epitope tag and a BirA\* sequence. pEGFP-N1 was obtained from Clontech and human AR was subcloned into pEGFP-C1 (Clontech) in fusion with a N-terminal GFP protein tag. Human KLF4 (NCBI clone NP004226.3) was subcloned into pMSCVpuro (Clontech) with an N-terminal 3xFLAG tag. All inserts were fully sequenced and protein expression was verified by western blot. Adenoviral plasmids for PSEBC-TSTA were previously described (29) and transfected into HEK293T cells for adenovirus production. Titers were determined using the Adeno-X Rapid Titer Kit (Clontech, Mountain View, CA, USA).

The DsiRNA catalog numbers and sequences were as follows (Integrated DNA Technologies, Coralville IA, USA): DsiAR (HSC.RNAI.N000044.12.1\_1 nm; #134941205 and HSC.RNAI.N000044.1 2.8\_2 nm; #134941208), DsiKLF4 (hs.Ri.KLF4.13.1; #153062069 and hs.Ri.KLF4.13.2; #153062072), DsiGRHL2 (hs.Ri.GRHL2.13.2; #153062024 and hs.Ri.GRHL2.13.3; #153062027), DsiMAML (hs.Ri-MAML1.13.1; #153062066 and hs.Ri.MAML1.13.2; #153062076), DsiRBPJ (hs.Ri.RBPJ.13.2; #153062030 and hs.Ri.RBPJ.13.3; #153062033), and DsiTBL1X (hs.Ri.TBL1X.13.1; #153062060 and hs.Ri.TBL1X.13.2; #153062063).

Targets	Reverse sequence	Forward sequence
siAR#1	rGrCrCrUrUrArArArUrCrUrGrUrGrArUrGrArUrCrCrUCA	rUrGrArGrGrArUrCrArUrCrArCrArGrArUrUrArArGrCrArU
siAR#2	rCrUrGrUrUrArUrArArCrUrCrUrGrCrArCrUrArCrUrCrCTC	rGrArGrGrArGrUrGrUrGrCrArGrArGrUrUrArArArCrArGrCrC
siKLF4#1	rArGrCrArCrUrArCrArArUrCrArUrGrUrCrArGrUrUCC	rGrGrArArCrUrUrGrArCrCrArUrGrArUrUrGrUrGrCrUrUrU
siKLF4#2	rGrUrUrCrUrArArArGrGrUrArCrCrArArArCrArGrGrAAG	rCrUrUrCrCrUrUrGrUrUrUrGrGrUrArCrCrUrUrUrArGrArCrCrA
siGRHL2#1	rGrArGrCrUrUrArArUrArCrGrArUrUrGrGrArArArCrATT	rArArUrGrUrUrUrCrCrArArUrCrGrUrArUrUrArArGrCrUrCrUrC
siGRHL2#2	rUrUrUrCrArUrCrUrUrGrGrArArUrUrGrGrUrUrUrCrUrAAA	rUrUrUrArGrArArCrCrArArUrUrCrCrArGrArUrGrArCrArUrC
siMAML1#1	rCrUrGrUrUrGrArArArCrUrUrUrArGrArUrArGrCrArGrAAT	rArUrUrCrUrGrCrUrArUrCrUrArArArGrUrUrUrCrArCrArGrArA
siMAML1#2	rCrGrCrArUrCrUrUrCrArUrGrArUrArCrArGrUrUrArGrGAG	rCrUrCrUrUrArArCrUrGrUrArUrCrArUrGrArGrArUrGrCrGrUrG
siRBPJ#1	rGrCrArUrUrUrArCrCrUrUrArArGrGrArUrArCrArGrAAA	rUrUrUrCrUrGrUrArUrCrCrUrArArGrGrUrUrArArArArGrCrArC
siRBPJ#2	rGrCrArUrGrCrUrCrUrArCrGrCrArUrUrCrArGrUrCrCrUTA	rUrArArGrGrArCrUrGrArArUrGrCrGrUrArGrArGrCrArUrGrCrUrG
siTBL1X#1	rCrArUrUrUrGrUrUrUrCrArArGrArGrArArUrCrArACA	rUrGrUrUrGrArUrUrCrUrCrUrUrGrArArArCrArArUrGrArG
siTBL1X#2	rUrCrArGrUrCrArUrArArUrCrArCrGrCrGrArArGrCrCAA	rUrUrGrGrCrUrUrCrGrCrGrUrGrArUrUrArUrUrGrArCrUrGrArUrU

Nontargeting DsiRNAs provided by the manufacturer were used as negative controls.

*Cell Culture and Transfection*

LNCaP and VCaP cells were obtained from ATCC. LAPC4 cells were kindly provided by Dr C. Sawyers. LNCaP were cultured in RPMI 1640 media containing 10% fetal bovine serum (FBS), LAPC4 and VCaP cells were cultured in DMEM media containing 10% FBS. Cell lines were tested for *mycoplasma* using the MycoAlert *Mycoplasma* Detection kit (Lonza, Basel, Switzerland). Transfections were performed using Lipofectamine 2000 (Thermo Fisher Scientific). Stable LAPC4 cells were selected with puromycin (5 µg/ml) for 1 month. Individual clones were picked and selected based on transgene expression. DsiRNAs (5 nM) were transfected using Lipofectamine 2000 (Thermo Fisher) following manufacturer’s guidelines.

*Cell Lysis and BioID Proximity Labeling*

For BioID experiments, LAPC4 cells were seeded at 50% confluence in four 15 cm tissue culture dishes per condition and grown for 24 h prior to treatments. Cells were treated with DHT (10 nM) for 0 h, 24 h, or 72 h. Biotin (50 µM) was added for the last 24 h prior to cell lysis. Cells were washed twice with PBS, then scrapped in PBS buffer before lysis in ice-cold RIPA buffer followed by benzonase (Sigma-Aldrich) treatment for 1 h and three cycles of sonication. Protein concentration was measured and normalized using a BCA kit (Thermo Fisher Scientific). Lysates were incubated under agitation for 3 h at +4 °C with 30 µl streptavidin agarose beads (Sigma-Aldrich). Beads were washed three times with lysis buffer. For MS experiments, beads were additionally washed twice with 20 mM Tris pH 7.4, and proteins were eluted by incubation with agitation at +4 °C with 50 mM H<sub>3</sub>PO<sub>4</sub> before digestion with trypsin, as described (30). A stage-tip purification step through a C18 column was performed in order to desalt further protein samples (31). Proteins were eluted in 0.5% acetic acid: 80% acetonitrile.

For western blotting experiments, cells were washed once with PBS and lysed in 1x Laemmli buffer. Whole-cell lysates were normalized based on their protein concentration, as assessed by BCA assay.

*Affinity Purification*

A total of 5 x 10<sup>6</sup> HEK293T cells were seeded in 10 cm tissue culture dishes and grown for 24 h. Cells were transiently transfected using polyethylenimine (PEI) with pEGFP-N1 or pEGFP-C1-AR to achieve similar levels of purification for GFP or GFP-AR and cotransfected with pMSCV(puro)-3xFLAG-KLF4. Cells were scrapped into IP buffer (50 mM Tris-HCl, pH 7.9, 1 mM EDTA, 0.1 mM EGTA, 12.5 mM MgCl<sub>2</sub>, 400 mM NaCl, 20% glycerol, 1% Triton X-100 (BioShop, Burlington, ON) containing protease (P8340, Sigma-Aldrich) and phosphatase inhibitors (Cocktail 2, Sigma-Aldrich). Cell lysates were kept on ice for 15 min and then sonicated 30 s at a low intensity. Cell lysates were cleared by centrifugation at 20,000 g for 1 min, and purifications were performed with 5 µl of GFP-Trap Agarose beads (Chromotek, New York) for 2h at +4°C. Beads were washed twice with IP buffer. Precipitates were recovered after 2 h of incubation on a rotating machine at +4°C and washed three times 10 min in IP buffer. Precipitates and total cell lysates were separated by SDS-PAGE and

transferred to nitrocellulose membranes prior to western blotting with the indicated antibodies.

*Western Blotting and Antibodies*

A total of 10–20 µg of whole-cell lysates was resolved by SDS-PAGE and transferred to nitrocellulose membranes (GE Healthcare). Loading of each track was verified with Ponceau S (Sigma-Aldrich) staining. Antibodies used were as follows: mouse anti-AR (Santa Cruz, #7305), rabbit anti-AR (Santa Cruz, #816), rabbit anti-KLF4 (Abcam, #215036), mouse anti-tubulin (Cell Signaling Technology, #3873), mouse anti-actin (Cell Signaling Technology, #3700), anti-GFP (Abcam, #290), rabbit anti-MED1 (Bethyl, #A300–793A), rabbit anti-MED12 (Bethyl, #A300–774A), rabbit anti-KMT2A (Bethyl, #A300–087A), mouse anti-DMAP1 (Santa Cruz, #373949), rabbit anti-POLH (Bethyl, #A301–231A), rabbit anti-NIPBL (Bethyl, #A301–779A), or mouse H3 (Cell Signaling Technology, #3638). Secondary antibodies were the following: anti-FLAG M2 (Sigma-Aldrich), horse anti-mouse HRP-linked IgG (Cell Signaling Technology, #7076), goat anti-rabbit HRP-linked IgG (Cell Signaling Technology, #7074), or streptavidin-HRP (Life Technologies #434323). Signal was revealed using BioRad Clarity Western ECL substrate and detected either on Hyblot CL autoradiography films (Denville) or with an Amersham Imager 600RGB (GE Healthcare). Signal quantification was performed using Image J software gel analysis tools (NIH).

*Luciferase Assay*

LAPC4 (1.0 x 10<sup>5</sup> cells/well), LNCaP (1.0 x 10<sup>5</sup> cells/well), and VCaP (1.6 x 10<sup>5</sup> cells/well) were seeded in 24-well plates with media containing 5% charcoal stripped FBS and grown for 18 h before PSEBCTSTA (3.5 MOI) adenovirus infection, DsiRNA transfection, and treatment with vehicle (EtOH) or DHT (10 nM). Seventy-two hours following infection, cells were washed once with HBSS and lysed. Luciferase assay was performed following manufacturer guidelines (Promega) with 20 µL of each lysate. Relative luminescence unit (RLU) was normalized by protein content in each well (normalized RLU = total-RLU/total protein amount). Protein concentration was estimated by adding 250 µl of Bradford reagent (ThermoFisher Scientific) to 3 µl of total lysate. Absorbance was measured using an Infinite F50 absorbance microplate reader (Tecan, Mannedorf, Switzerland) at 595 nm.

*RT-qPCR Assay*

LAPC4 (6 x 10<sup>5</sup> cells/well) cells were seeded in 6-well plates with DMEM medium containing 5% charcoal stripped FBS, transfected with DsiRNAs, and grown 24 h before vehicle/DHT treatment. Cells were washed twice with PBS, and total RNA was extracted using TriPure reagent (Sigma), according to the manufacturer’s recommendations. RNAs were cleaned using the GeneJET RNA purification kit (Thermo Fisher Scientific). Reverse transcription was performed using 2.5 µg of total RNA according to the standard SuperScript VIL0 Master Mix (Invitrogen). The resulting cDNAs were diluted at 1/24 and then 10 µL was used in a quantitative PCR reaction carried out with the SYBR Select Master Mix (Applied Biosystems). *Actin* was used for normalization of RT-qPCR data. Fold changes in mRNA expression levels were calculated using the comparative Ct method.

The following primers were used:

Targets	Reverse sequence	Forward sequence
AR	CTGATGCAGCTCTCTCGC	CCCACATCCTGCTCAAGACG
KLF4	GGGCCCAATTACCCATCCTT	GGCATGAGCTCTTGGTAATGG
PSA	CCTCACAGCTACCCACTGCA	GATGAAACAGGCTGTGCCG
Actin	GCCCACATAGGAATCCTTCTGAC	AGGCACCAGGGCGTGAT

*Immunofluorescence and Microscopy*

LNCaP cells were starved overnight, then transfected with DsiRNAs for 48 h. Cells were fixed in ice-cold methanol for 4 min at  $-20^{\circ}\text{C}$  after 4 h of stimulation with DHT (10 nM). This was followed by three washes with PBS and incubation with the following antibodies diluted in blocking buffer (0.2% BSA (Bioshop), 0.1% Triton X100 (Sigma-Aldrich)): rabbit anti-FLAG (Sigma Aldrich, #F7425), mouse anti-AR (Santa Cruz, #7305), or rabbit anti-KLF4 (Abcam, #215036) for 1 h at room temperature. After washes in PBS, coverslips were incubated with Alexa 568-conjugated goat anti-rabbit (Thermo Fisher Scientific, #A11011) or Alexa 488-conjugated goat anti-mouse (Cell Signalling Technology, #4408) antibodies for 1 h at room temperature. They were washed twice with PBS before being mounted on slides using Pro-Long Gold antifade with DAPI (Thermo Fisher). Pictures were acquired with an Olympus FV1000 using the Fluoview 3.0 software or with a Nikon Eclipse E600 imaging system using MetaView.

*Experimental Design and Statistical Rationale*

Each BioID experiment was performed in biological triplicate. Controls for each experiment were treated concomitantly to experimental samples. 3xFLAG-BirA\* with and without biotin and 3xFLAG-BirA\*-AR without biotin were used as controls. The highest total spectra number from any of the three controls was utilized as the control value for SAINT analysis. Biological triplicates were required and sufficient to perform SAINT analyses to distinguish background from *bona fide* protein associations (32). Statistical analyses were performed via two-way ANOVA using Prism version 7 (GraphPad software inc California, USA). *p* values  $<0.05$  were considered significant.

*Mass Spectrometry*

Samples were analyzed by nanoLC/MSMS. For each injection, 1  $\mu\text{g}$  of peptide samples was injected and separated by online reversed-phase (RP) nanoscale capillary liquid chromatography (nanoLC) and analyzed by electrospray mass spectrometry (ESI MS/MS). Experiments were performed with a Dionex UltiMate 3000 nanoRSLC chromatography system (Thermo Fisher Scientific/Dionex Softron GmbH) connected to an Orbitrap Fusion mass spectrometer (Thermo Fisher Scientific) driving with Orbitrap Fusion Tune Application 2.0 and equipped with a nanoelectrospray ion source. Peptides were trapped at 20  $\mu\text{l}/\text{min}$  in loading solvent (2% acetonitrile, 0.05% TFA) on a 5 mm  $\times$  300  $\mu\text{m}$  pepmap cartridge precolumn (Thermo Fisher Scientific/Dionex Softron GmbH) during 5 min. Then, the precolumn was switched online to a house-made 50 cm  $\times$  75  $\mu\text{m}$  internal diameter separation column packed with ReproSil-Pur C18-AQ 3- $\mu\text{m}$  resin (Dr Maisch HPLC GmbH, Ammerbuch-Entringen), and the peptides were eluted with a linear gradient from 5 to 40% solvent B (A: 0.1% formic acid, B: 80% acetonitrile, 0.1% formic acid) in 60 min at 300 nL/min. Mass spectra were acquired using a data-dependent acquisition mode using Thermo XCalibur software version 3.0.63. Full-scan mass spectra (350–1800 *m/z*) were acquired in the orbitrap using an AGC target of 4e5, a maximum injection time of 50 ms, and a resolution of 120,000. Internal calibration using lock mass on the *m/z* 445.12003 siloxane ion was used. Each MS scan was followed by acquisition of fragmentation MSMS spectra of the most intense ions and with a minimum intensity threshold of 5000 for a total cycle time of 3 s (top speed mode). The selected ions were isolated using the quadrupole analyzer in a window of 1.6 *m/z* and fragmented by higher-energy collision-induced dissociation (HCD) with 35% collision energy. The resulting fragments were detected by the linear ion trap in rapid scan rate with an AGC target of 1e4 and a maximum injection time of 50 ms. Dynamic exclusion of previously fragmented peptides was set for a period of 20 s and a tolerance of 10 ppm.

All MS/MS peak lists (MGF files) were generated using Thermo Proteome Discoverer software (Thermo Fisher Scientific Inc, version 2.1.0). MGF sample files were then analyzed using Mascot (Matrix Science, London, UK; version 2.5.1). Mascot was set up to search the Uniprot Complete Proteome *Homo sapiens* database (92,237 entries, February 2017 release) assuming the digestion enzyme trypsin. Mascot was searched with a fragment ion mass tolerance of 0.6 Da and a parent ion tolerance of 10 ppm. Carbamidomethylation of cysteines was set as fixed modification and oxidation of methionine, deamidation of asparagine and glutamine, and phosphorylation on serine, threonine, and tyrosine were specified as a variable modification. Two missed cleavages were allowed.

Scaffold (version 4.8.1), Proteome Software Inc, Portland, OR) was used to validate MS/MS-based peptide and protein identifications. Proteins/peptides FDR rate was set to 1% or less based on decoy database searching. Protein probabilities were assigned by the Protein Prophet algorithm (33). Proteins that contained similar peptides and could not be differentiated based on MS/MS analysis alone were grouped to satisfy the principles of parsimony. Interaction networks were modeled using Cytoscape v3.1.1.

*Chromatin Immunoprecipitation Coupled with Massively Parallel DNA Sequencing (ChIP-seq)*

ChIP-seq experiments were performed as described previously (34–36). Briefly, 50 million of LAPC4 cells treated for 1h with vehicle (EtOH) or DHT (100 nM) were cross-linked for 10 min with 1% formaldehyde and quenched with 125 mM glycine for 5 min. Cells were then washed with PBS, pelleted, flash frozen, and stored at  $-80^{\circ}\text{C}$ . Sonicated DNA fragments were immunoprecipitated with antibodies directed against KLF4 (R&D Systems, AF3640) and AR (Sigma, EMB Millipore, #06–680). Library preparation and high-throughput sequencing were performed at the next-generation sequencing platform of Centre de Recherche CHU de Québec (CRCHUQ), Québec, Canada. Analysis of raw sequencing reads was performed using the MUGQIC ChIP-Seq pipeline (37). Briefly, reads were trimmed for adaptor sequences using Trimmomatic (38). High-quality reads were aligned to the human reference genome (hg38) with BWA aligner (39). PCR duplicates were removed with picard MarkDuplicates (<http://broadinstitute.github.io/picard/>). Narrow peaks were called using MACS2 callpeak (40), supplying the sequenced corresponding input DNA as background control. Narrow peaks found in all replicates were used as the list of enriched regions. To generate genomic visualizations, samples from pairs of replicates were pooled. Reads from BAM files were extended to 225 bp and normalized using bins per millions mapped reads (BPM) method and a bin size of 10 bases with bamCoverage function from deepTools (41). BPM (per bin) = number of reads per bin/sum of all reads per bin (in millions). ChIP-Seq heatmaps were generated using computeMatrix and plotHeatmap functions from deepTools. Tracks images were generated using the University of California, Santa Cruz (USCS) Genome Browser (42).

## RESULTS

*BioID Proximity Labeling Identifies Known and Novel AR-associated Proteins*

To establish cell lines relevant to AR function, we selected LAPC4 prostate cells, which express a wild-type AR (43, 44). We generated clonal LAPC4 lines stably expressing AR fused to 3xFLAG-BirA\* at levels similar to endogenous AR (Fig. 1A). To determine whether the BirA\*-AR fusion was functional, we analyzed its subcellular compartmentalization following stimulation with its ligand, DHT. We found that DHT stimulation led

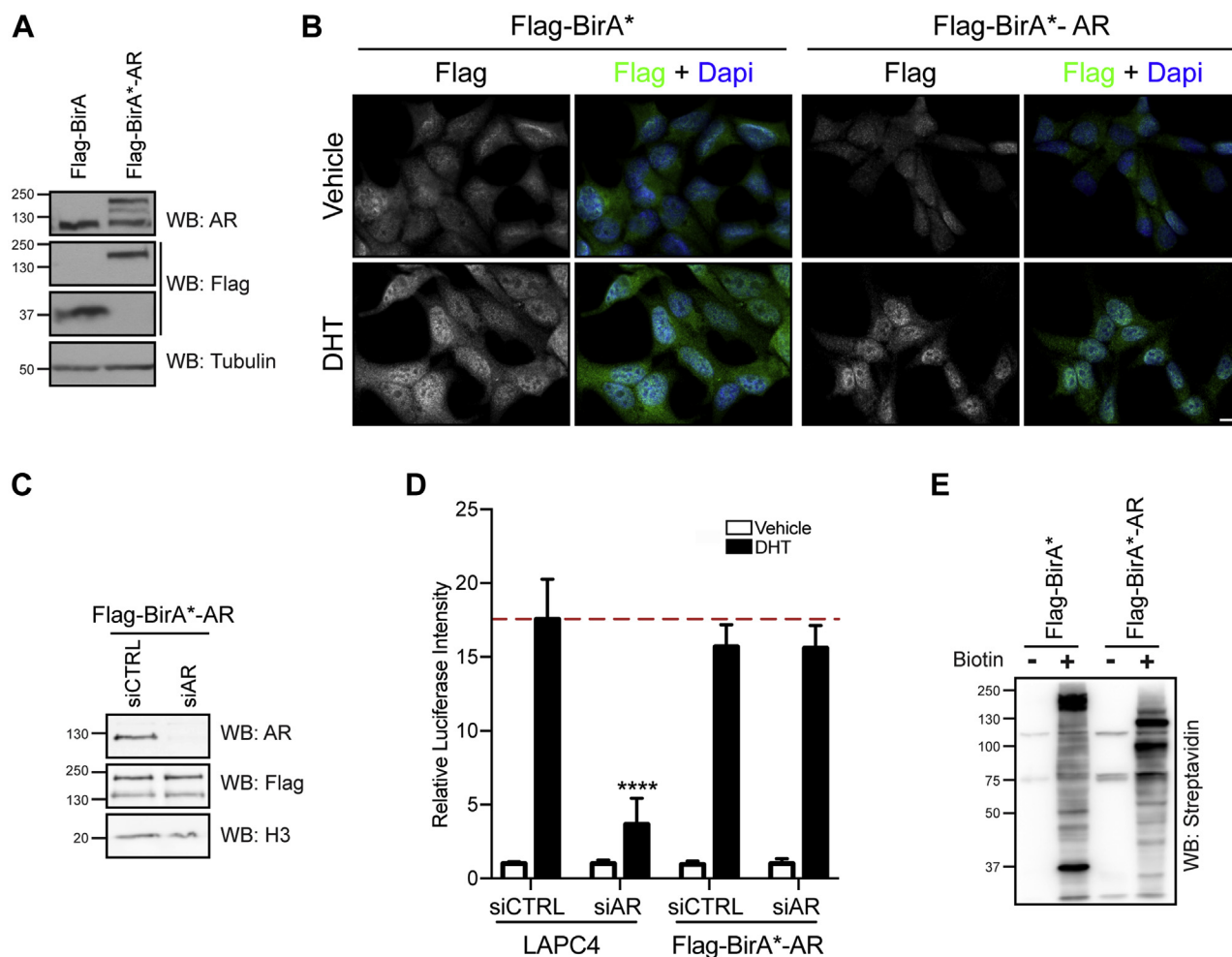


**FIG. 1. LAPC4 stable cell lines express a functional Flag-BirA\*-AR chimera.** *A*, Clonal LAPC4 stable cell lines expressing either BirA\* or BirA\*-AR Flag fusion proteins were analyzed by western blot to evaluate transgene expression. *B*, Flag-BirA\*-AR expressing LNCaP cells were analyzed by immunofluorescence in the presence or absence of 10 nM DHT (scale bar: 10  $\mu$ m). *C*, Flag-BirA\*-AR LAPC4 cells were depleted of endogenous AR using siRNA. Silencing efficiency was assessed by western blot. *D*, Parental (control) and Flag-BirA\*-AR LAPC4 cells were depleted of endogenous AR using siRNA, infected with a luciferase reporter gene coupled with a PSA promoter, and treated with a vehicle or 10 nM DHT. Luciferase activity was normalized to the total protein amount for each sample and to the vehicle-treated condition to obtain relative luciferase intensities for each sample. Mean values and standard deviation from three independent experiments are presented. (\*\*\*\*  $p \leq 0.0001$ ). *E*, endogenous proteins were biotinylated by Flag-BirA\* and Flag-BirA\*-AR after 24h of biotin addition to the culture media, as detected by binding to streptavidin. Blots in *A*, *C*, and *E* are representative of three independent experiments.

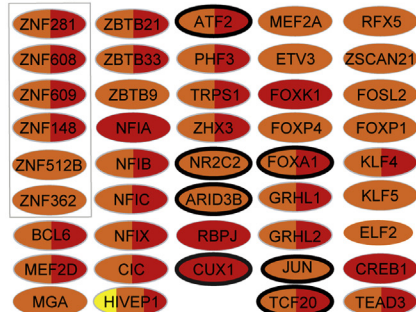
to nuclear accumulation of 3xFLAG-BirA\*-AR, as it did for wild-type AR, in LNCaP cells (Fig. 1B). To further support this, we tested if 3xFLAG-BirA\*-AR could substitute endogenous AR function in LAPC4 cells. Using a luciferase PSA reporter assay (45, 46), we found that 3xFLAG-BirA\*-AR restored transcription in AR-depleted cells (Fig. 1, C-D). In addition, we validated that addition of biotin to LAPC4 cells expressing 3xFLAG-BirA\*-AR induced a strong biotinylation pattern (Fig. 1E). Together, these observations suggest that 3xFLAG-BirA\*-AR recapitulates endogenous AR functions.

To delineate the AR proximity network, we affinity-purified biotinylated proteins following the addition of biotin to 3xFLAG-BirA\*-AR and 3xFLAG-BirA\* LAPC4 cell cultures and identified them using MS. We treated cells with DHT or vehicle

for 24h or 72h (47, 48) and performed experiments in biological triplicate. We eliminated nonspecific interactions *via* SAINTexpress (49), using 3xFLAG-BirA\*-expressing cells as controls (supplemental Table S1). Only high-confidence interactions (SAINT score  $\leq 0.9$ ) were considered for follow-up experiments and analyses (supplemental Fig. 1A). We identified 31 proteins associated with AR in the absence of agonist (Fig. 2, supplemental Table S1). Strikingly, we also found that 182 and 200 (261 nonredundant) proteins were associated with AR upon stimulation with DHT for 24h or 72h, respectively, despite the loss of six proteins from the 31 detected under nonstimulated conditions. While most of the AR-associated proteins were identified exclusively in DHT-stimulated cells, a few components of the BAF

**Transcription factors**

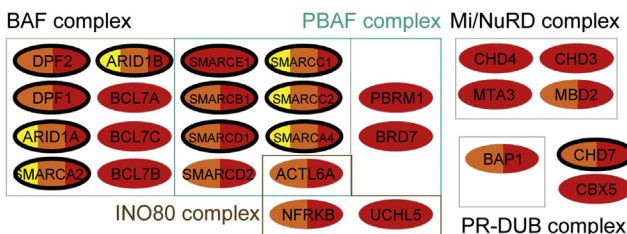
Zinc finger family



**Chromatin organization**

UBN2, TNRC18

**Chromatin remodeling**

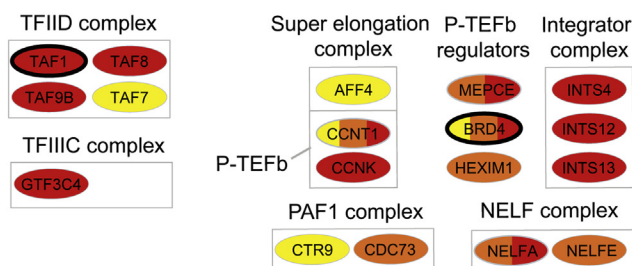


**Chromatin 3D organization**

cohesin complex regulators: NIPBL, WAPL

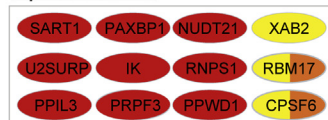
**RNA Pol II transcription machinery**

**Transcription initiation**    **Transcription elongation**



**RNA processing**

**Spliceosome**



**mRNA cleavage and polyadenylation**

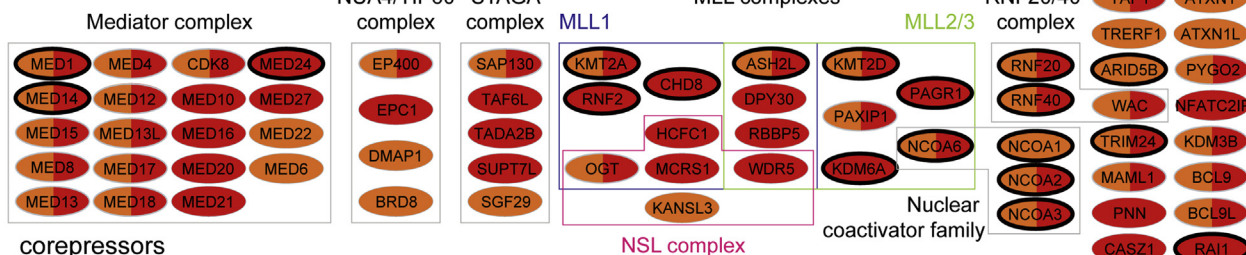


**RNA binding protein**

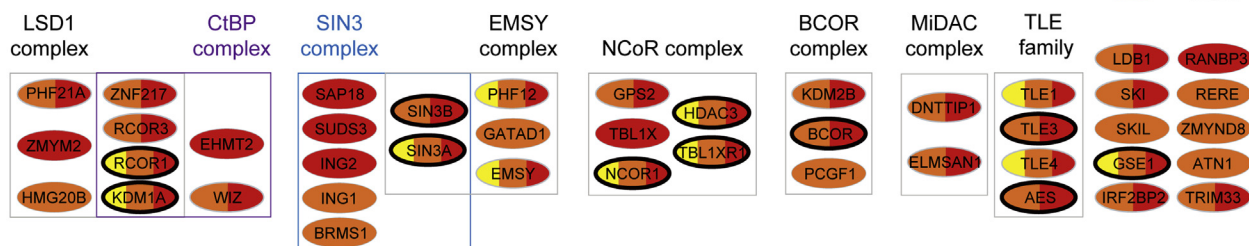


**Transcriptional cofactors**

**coactivators**



**corepressors**



**DNA metabolism**

**DNA replication**

ORC2, WRNIP1

**DNA methylation**

SMCHD1, TET2

**DNA repair**

MDC1, POLH, SSBP2, USP7, USP28

**Cell cycle regulation**

LIN complex: LIN9, LIN54, KIFC1, KNL1, ANLN, HIRA, CHAMP1, KIF4A, CDCA2, TPX2

**DNA binding**

AHDC1, SCML2

**Other partners**

QSER1, CSNK2A1, c16orf87, LENG8, PRR12, YLPM1, MORC4, TXNL1, PRRC2B, CSNK2B, FBRS, MRPS9

Legend: Yellow circle = Unstimulated, Orange circle = DHT 24h, Red circle = DHT 72h, Black circle = Known

FIG. 2. **BioID proximity labeling reveals known and novel AR-associated proteins.** Flag-BirA\* and Flag-BirA\*-AR expressing cells were stimulated for 24h (orange), 72h (red) with 10 nM DHT or vehicle (yellow) to perform BioID. The AR proximity interaction landscape displays previously reported interactions (known) from the BioGRID, GSP-Prot, and IntAct databases (circled in black). Proteins were grouped relative to their functions according to CORUM and GeneCards databases.

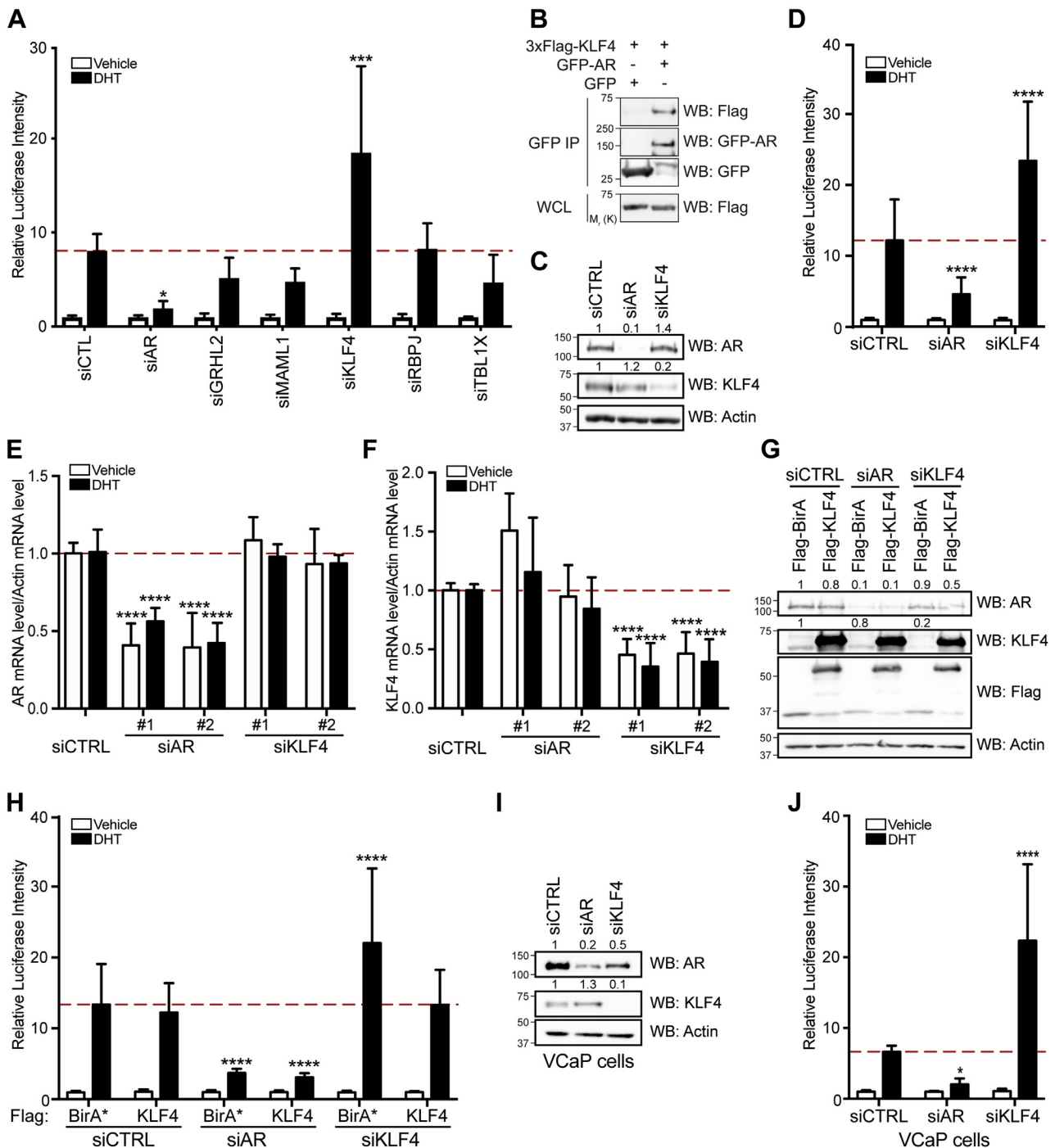


**FIG. 3. KLF4 depletion does not affect AR expression but increases its transcriptional activity.** A, control, siAR, siGRHL2, siMAML1, siKLF4, siRBPJ, and siTBL1X transfected LAPC4 cells were infected with a luciferase reporter gene coupled with a PSA promoter and treated with a vehicle or 10 nM DHT. Luciferase activity was normalized to the total protein amount for each sample and to the vehicle-treated condition to obtain relative luciferase intensities for each sample ( $*p \leq 0.05$ ;  $***p \leq 0.001$ ). B, western blot analysis of 3xFLAG-KLF4 following GFP affinity purification in HEK293 T cells cotransfected with GFP/GFP-AR and 3xFLAG-KLF4. C–D, Control, siAR, or siKLF4 transfected LAPC4 cells were infected with a luciferase reporter gene coupled with a PSA promoter and treated with a vehicle or 10 nM DHT. Normalization was performed as in (A). Endogenous AR- or KLF4-depleted cells were analyzed by western blot (C) to confirm protein depletion. E and F, Control, siAR, or siKLF4 transfected LAPC4 cells were stimulated with a vehicle or 10 nM DHT, and RT-qPCR was performed to assess AR (E) and KLF4 (F) mRNA levels. Data was normalized to actin mRNA levels, and then to the control condition to obtain relative values. G and H, Control, siAR, or siKLF4 transfected LAPC4 cells were infected with a luciferase reporter gene coupled with a PSA promoter, transfected with Flag-BirA or Flag-KLF4, and treated with a vehicle or 10 nM DHT. Endogenous AR- or KLF4-depleted LAPC4 cells were analyzed by western blot (G) to determine protein



(SMARCA2/4, SMARCC1/2) and NCoR (NCOR1, HDAC3, TBL1XR1) complexes were identified in nonstimulated cells. Among the DHT-dependent associations, we found 54 proteins previously described to associate with AR according to the BioGRID (22), GSP-Prot (23) and IntAct databases (24), including NCOA3/SRC3 (50), SMARCD1 (27), TCF20/SPBP (28) and RNF20 (51). Interestingly, we identified 213 proteins whose association with AR was not reported in databases. We performed affinity purification of GFP or GFP-AR in HEK293 cells and confirmed the interaction between AR and endogenously expressed candidates MEDiator complex subunit 1 (MED1), MEDiator complex subunit 12 (MED12), Lysine Methyltransferase 2A (KMT2A), DNA Methyltransferase 1 Associated Protein 1 (DMAP1), DNA Polymerase eta (POLH), and NIPBL cohesion loading factor (NIPBL) (supplemental Fig. 1, B–G). Therefore, this data set meaningfully confirms and expands the number of reported AR-associated proteins according to the BioGRID, GSP-Prot, and IntAct databases.

To depict the extent of our AR proximity network, we manually classified components into groups according to their function (Fig. 2). Strikingly, our analysis revealed a DHT-dependent association between AR and a number of transcription factors. This is consistent with the observation that nuclear receptors may trigger binding of clusters of transcription factors, as shown for the glucocorticoid receptor (52). This analysis also highlighted a number of transcriptional coactivators, including previously characterized RNF20-RNF40 (51), members of the NCoA/SRC family (53, 54), and most components of the mediator complex (supplemental Fig. 1, B–C) (55, 56). In addition, we further exposed other transcriptional cofactors and corepressors, as well as components of functional protein complexes involved in chromatin organization (NIPBL (supplemental Fig. 1G); BAF, NuRD complexes), transcription initiation (TFIID), cell cycle regulation (LIN complex), or RNA processing (spliceosome) (Fig. 2). Together, the AR proximity network obtained from LAPC4 cells delineates a significant number of known and new AR-associated proteins that play multiple roles in the regulation of gene expression, as well as other cellular processes.

#### *KLF4 Acts as a Repressor for the AR Target Gene KLK3 (PSA)*

To investigate the function of these new AR-associated proteins, we selected five candidates (*i.e.*, GRHL2, KLF4, MAML1, RBPJ, TBL1X) based on SAINT score and gene expression in prostate (supplemental Table S1) (57). Using the

luciferase PSA reporter assay, we tested whether their depletion in LAPC4 cells led to changes in AR-dependent transcriptional regulation. As expected, cells depleted of AR showed a significant decrease in luciferase signal following DHT stimulation relative to control cells ( $p \leq 0.05$ , two-way ANOVA), thus confirming the validity of our assay (Fig. 3A). KLF4 depletion surprisingly led to a stronger activation of the AR-driven luciferase reporter in DHT-stimulated LAPC4 cells (Fig. 3A). While the depletion of the four other AR-associated candidates that we tested did not lead to statistically significant changes, it did induce in most cases a slight decrease in AR reporter activation. We confirmed by coexpression and affinity purification that KLF4 associates with AR (Fig. 3B), reinforcing our BioID proximity labeling results and supporting a role for KLF4 in regulating PSA transcription, as suggested by our luciferase PSA reporter assays (Fig. 3A). We further found that in KLF4-depleted cells, DHT stimulation increased AR-driven luciferase reporter signal by at least 1.7-fold, while cells depleted of AR displayed a 3.7-fold decrease ( $p \leq 0.0001$ ) (Fig. 3, C and D). Interestingly, KLF4 was previously reported to directly bind to the AR promoter and KLF4 depletion to decrease AR protein levels in LNCaP cells, which express a mutated AR (58). To determine whether KLF4 knockdown affected endogenous wild-type AR expression in LAPC4 cells, we analyzed mRNA levels *via* RT-qPCR. We found that AR RNA levels were unchanged in KLF4-depleted cells relative to controls, both in nonstimulated and in DHT-stimulated cells (Fig. 3E). We also observed that AR protein expression was unaffected (Fig. 3C). Consistent with this observation, ectopic 3xFLAG-KLF4 expression did not lead to increased AR levels (Fig. 3G). We detected a slight increase in KLF4 expression in AR-depleted cells with one of the two siRNAs targeting AR (Fig. 3F); however, this was not confirmed at the protein level (Fig. 3C).

To confirm that the PSA reporter repression was due to KLF4 loss-of-function, we re-expressed 3xFLAG-tagged KLF4 that is not affected by siRNAs, which both target the 3'UTR sequence. Re-expression of 3xFLAG-KLF4, but not 3xFLAG-BirA\*, decreased luciferase levels to those of control LAPC4 cells in the presence of DHT (Fig. 3, G and H). Cells transfected with siCtrl or siAR did not display a change in luciferase levels following 3xFLAG-KLF4 re-expression compared with controls. To corroborate our findings in another prostate cell line that expresses wild-type AR, we opted for VCaP cells (59). We confirmed that AR-dependent transcription of the luciferase transgene was increased following DHT stimulation and

---

levels. Luciferase activity was normalized to the total protein amount for each sample and to the vehicle-treated condition to obtain relative luciferase intensities for each sample (H). I and J, control, siAR, or siKLF4 transfected VCaP cells were infected with a luciferase reporter gene coupled with a PSA promoter and treated with a vehicle or 10 nM DHT. Endogenous AR- or KLF4-depleted cells were analyzed by western blot (I) to confirm protein depletion. Luciferase activity was normalized to the total protein amount for each sample and to the vehicle-treated condition to obtain relative luciferase intensities for each sample (J). D, E, F, H, J, Mean values and standard deviation from three independent experiments are presented (\* $p \leq 0.05$ ; \*\*\*\* $p \leq 0.0001$ ). Blots in B, C, and G are representative of three independent experiments, blots in I are representative of two independent experiments.

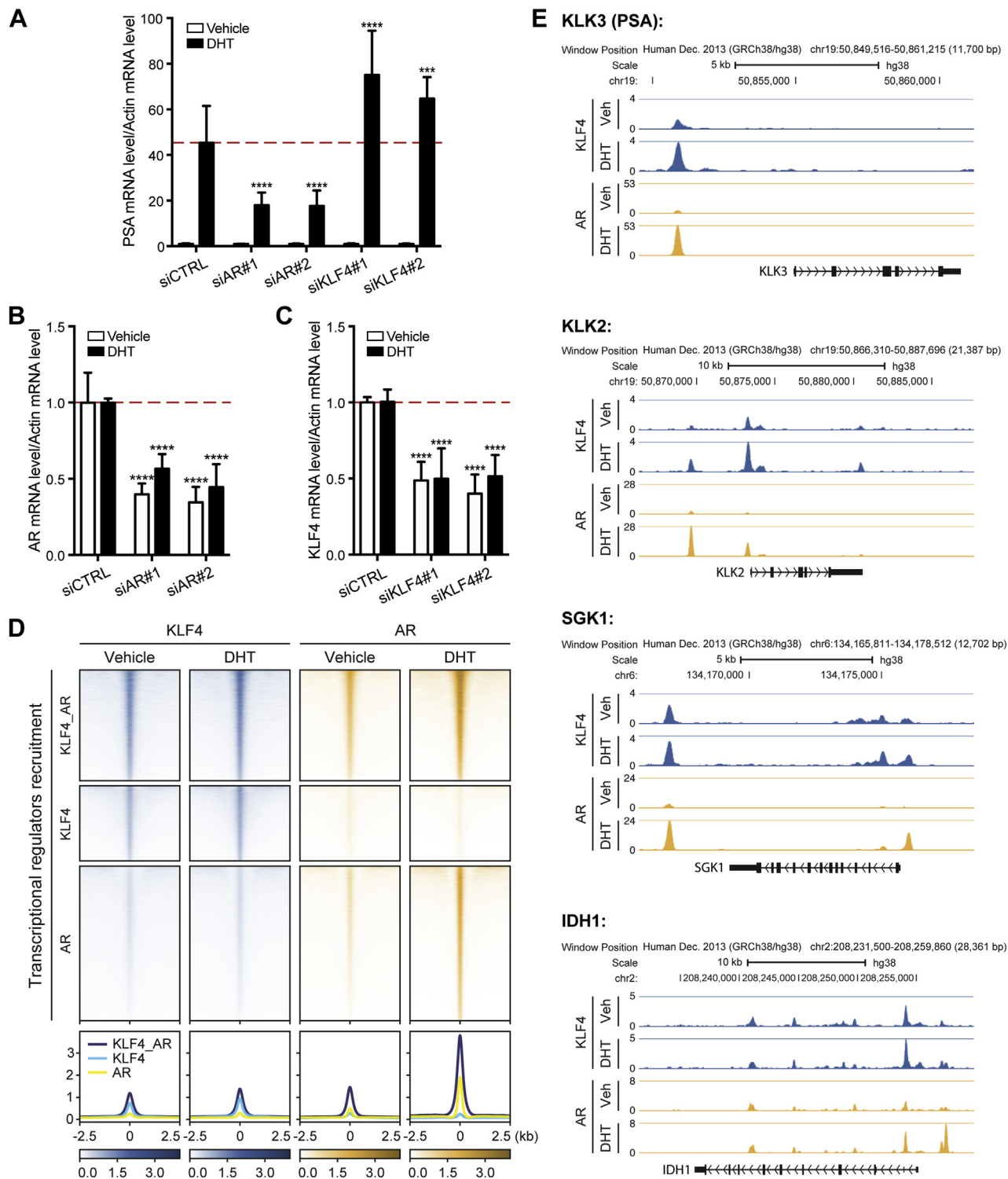


**FIG. 4. A large fraction of KLF4 colocalizes with AR in the genome and acts as a repressor of the AR target gene *KLK3* (*PSA*) in LAPC4 cells.** A–C, control, siAR, or siKLF4 transfected LAPC4 cells were stimulated with a vehicle or 10 nM DHT, and RT-qPCR was performed to assess PSA mRNA levels (A). AR (B) and KLF4 (C) depletion efficiency was also determined by RT-qPCR. Data was normalized to actin mRNA levels, and then to the control condition to obtain relative values. Mean values and standard deviation from three independent experiments are presented (\*\* $p \leq 0.001$ ; \*\*\*\* $p \leq 0.0001$ ). D, heat map showing the co-occupancy of KLF4 and AR across the genome of LAPC4 cells. Top: Density heat maps representing KLF4 and AR ChIP-seq intensities in the absence (control) or presence of DHT at three groups of genomics regions (occupied by AR and KLF4 ( $n = 35,709$ ), occupied by KLF4 only ( $n = 24,190$ ), and occupied by AR only ( $n = 49,877$ )). Regions were

that it was blocked in AR-depleted cells. Moreover, we showed that KLF4 knockdown led to a strong augmentation of luciferase levels, thus supporting the observations made in LAPC4 cells (Fig. 3, I and J). Taken together, our results suggest that AR and KLF4 are functional partners.

To validate that KLF4 acts as a repressor of the AR target gene *PSA* in an endogenous context, we performed RT-qPCR analyses of mRNA levels of *PSA*. Following DHT stimulation, *PSA* mRNA levels increased 45-fold in LAPC4 cells. This activation was hindered in AR-depleted cells, as *PSA* messengers decreased by 2.5-fold ( $p \leq 0.0001$ , two-way ANOVA) (Fig. 4, A and B). As observed in the luciferase reporter assay, *PSA* mRNA increased significantly by an average of 1.5-fold ( $p \leq 0.0001$ , two-way ANOVA), following KLF4 knockdown with two independent siRNA sequences tested (Fig. 4, A and C). This latter increase in *PSA* expression was not due to an accumulation of AR in the nucleus (supplemental Fig. 2). Together, our data strongly support the idea that KLF4 acts as a repressor during androgen-dependent *PSA* gene activation.

To determine if AR and KLF4 shared cis-regulatory regions genome-wide, we surveyed their recruitment with/without a 1h DHT treatment using chromatin immunoprecipitation coupled with massively parallel DNA sequencing (ChIP-seq) in LAPC4 cells. As expected, the number of regions occupied by AR increased from 24,379 in control conditions to 85,312 when cells were stimulated with DHT. For KLF4, 26,891 regions were observed in control cells compared with 59,806 in DHT-stimulated cells (supplemental Table S3 and supplemental Fig. S3). Overall, when we considered the entire set of regions occupied by KLF4 and/or AR in all conditions, 33% were bound by both transcription factors (Fig. 4D). Interestingly, for regions co-occupied by KLF4 and AR, the signal densities for both transcription factors were correlated, thus supporting co-occupancy. In addition, as expected, signal density for AR increased following DHT stimulation while KLF4 was relatively stable. While many regions occupied by the AR following the DHT treatment were also occupied by KLF4 in control conditions, a similar fraction was not occupied (supplemental Fig. S3), suggesting different models for interactions between these two transcription factors. In total, we found 4097 genes with KLF4 and AR both binding at their promoter region following DHT stimulation (supplemental Table S4). Closer examination of density profiles of well-known AR target genes supported co-occupancy. For example, the well-characterized enhancer region of the *PSA* gene (*KLK3*) was occupied by both KLF4 and AR (Fig. 4E). Similar results were observed for *KLK2*, *SGK1*, and *IDH1*. Therefore, the ChIP-seq experiments

support subnuclear colocalization of KLF4 and AR, suggesting a functional association.

#### DISCUSSION

In this work, we report a high-confidence proximity network for AR in prostate cells. We found that the majority of network components associate with AR in a ligand-dependent manner. Strikingly, we further reveal 213 new proteins associated with AR. Recently, Lampiäinen *et al.* reported an AR proximity network comprised of 32 preys in HEK293 cells (20). We identified 24/32 proteins that these authors revealed in DHT-stimulated cells, as well as 237 additional DHT-dependent interactions. Discrepancies are likely attributed to the differences in cell lines used in the two studies, as well as biotin/DHT treatment durations, composition of controls for BioID experiments, and MS data analysis workflows. We propose that the higher complexity of the AR proximity network that we reveal here is due to higher endogenous expression of wild-type AR and responsiveness to androgens of LAPC4 versus HEK293 cells, as suggested by previous reports (21).

The AR proximity network that we uncovered outlines associations between AR and core components of the transcriptional and chromatin remodeling machineries, in addition to highlighting associations with proteins implicated in RNA processing, DNA metabolism, or DNA repair. For example, we identified 109 transcriptional cofactors, including components of the mediator complex and the NCoR complex. Moreover, we found a number of proteins previously described to be part of chromatin remodeling complexes such as BAF and NuRD. Many new interactors are subunits of protein complexes previously reported to associate with AR. This observation emphasizes the potential of BioID proximity labeling to identify proteins present in the vicinity of a given bait.

Of note, many interactors of AR found in the BioGRID, GSP-Prot, or IntAct database were not determined as high-confidence interactors in our analysis (supplemental Table S1), highlighting limitations of the BioID proximity labeling approach. For example, HSP90AA1 (Heat shock protein HSP90-alpha), HSP90AB1 (Heat shock protein 90-beta), HSPA1B (Heat shock 70 kDa protein 1B), HSPA2 (Heat shock-related 70 kDa protein 2), HSPA5 (Heat shock 70 kDa protein 5), and HSPD1 (60 kDa heat shock protein) were detected as AR proximity interactors, but they did not pass the high-confidence threshold due to their presence in the 3xFLAG-BirA\* controls (supplemental Table S1).

Using an affinity purification approach, we confirmed the previously reported association between AR and MED1 or

ranked according to the total read density in the KLF4 control condition. Color scales indicate bins per million mapped reads (BPM). Bottom: Average read density plots for the same groups of regions. A region of 5kb centered on the occupied region is displayed. E, ChIP-Seq occupancy profiles of KLF4 and AR in control and DHT-stimulated cells. Genome tracks show colocalization of KLF4 (blue) and AR (yellow) ChIP-Seq peaks in the neighborhood of *KLK3* (*PSA*), *KLK2*, *SGK1*, and *IDH1* genes that are known to be regulated by AR. ChIP-Seq profiles are displayed in BPM. Gene depictions are presented below the gene tracks.

KMT2A, but we also validated new interaction partners for AR (Fig. 3B and supplemental Fig. 1, B–G). Among those, we identified KLF4 as a new AR-associated protein. Interestingly, Siu *et al.* previously discovered the existence in LNCaP cells of a reciprocal feedback loop between KLF4 and AR, in which each protein binds to the promoter of each other's gene (58). This observation was confirmed in our ChIP-Seq data. However, in LAPC4 cells, we did not observe a change in AR expression or protein levels upon KLF4 knockdown, neither a change in KLF4 expression or protein levels in cells depleted of AR. Therefore, it remains possible that the self-reinforcing loop between KLF4 and AR is cell-type specific. However, we did observe a significant overlap genome-wide between regions occupied by KLF4 and AR. These observations underline the importance of further examining AR-associated proteins in several PCa cell lines harboring different genetic and proteomic landscapes to possibly extend findings to primary PCa.

KLF4 function in transcriptional regulation is considered to be context-specific (60, 61). For example, during induced reprogramming of somatic cells into pluripotent cells, KLF4 represses somatic genes in an early phase and subsequently activates pluripotency genes (62). Consistent with this latter role, we show that KLF4 represses the transcription of the AR target gene *PSA*, but exclusively yet consistently when cells are stimulated with DHT to activate AR. Interestingly, KLF4 was previously reported to directly associate with the DNA-binding region of ER $\alpha$ , thereby inhibiting the transcriptional activity of this nuclear receptor, in an estrogen-dependent manner (63). Our data with AR suggests a common mechanism for the regulation of nuclear receptor-dependent *PSA* gene regulation by KLF4.

Recently, Fei *et al.* reported a genome-wide CRISPR/Cas9 knockout screen to identify essential genes in LNCaP PCa cells (64). Among the top 1000 gene products (including AR) that they deemed essential, we identified 15 in our AR BioID experiments (supplemental Table S2). Interestingly, comparison of pathway information revealed a number of common functional groups (Fig. 2), including RNA processing, transcription initiation, and DNA replication. While the proteome landscape between LNCaP cells, which feature a mutated AR, and LAPC4 cells utilized in the BioID experiments may be different, the relatively low number of essential genes among the AR proximity interaction landscape suggests that most candidates could be successfully targeted to modulate AR activity in PCa cells and suggests novel possibilities of treatment for prostate cancer patients.

KLF4 has been associated with either oncogenic properties, such as in osteosarcoma (65), either with tumor suppressive functions, such as in the lung (66), gastric (66), and prostate cancers (67). For example, overexpression of KLF4 in T24 urothelial bladder carcinoma cells leads to p21 accumulation, G1-phase arrest, and a significant decrease of tumor growth in a xenograft model (68). It was also reported to decrease proliferation of colorectal cancer cells by repressing cyclin D1

transcription (69). In prostate cancer, *KLF4* transcription and KLF4 protein levels were decreased in metastases, while its re-expression inhibited prostate cancer cell migration and invasion (67). This suggested its potential usage as a prognosis marker. Our work proposing that KLF4 can impair AR adds another layer of complexity to KLF4 tumor suppressive function in controlling prostatic cell proliferation and survival. Moreover, this leads to the premise that simultaneous down-regulation of KLF4 with increased AR levels could indicate a less favorable prostate cancer prognosis.

Together, we provide a large, high-confidence proximity interaction network for AR obtained from androgen-responsive cells. We further demonstrate the relevance of our data by characterizing the codistribution of KLF4 and AR across the genome, as well as a key repressive function for KLF4 in the regulation of the AR target gene *PSA*.

#### DATA AVAILABILITY

The mass spectrometry proteomics data have been deposited to the ProteomeXchange Consortium *via* the PRIDE partner repository with the data set identifiers PXD011974 and 10.6019/PXD011974 (70).

The sequencing data generated for this publication is available on GEO (71), under accession number GSE161189.

*Supplemental data*—This article contains [supplemental data](#).

*Acknowledgments*—We thank members of the Bisson, Bilodeau, and Pouliot laboratories for plasmids and discussions, J. Y. Masson and J. Côté for antibodies, as well as E. Coyaud and B. Raught for constructs and advice. Mass spectrometry was performed at the CHU de Québec – Université Laval Proteomics Platform.

*Funding and additional information*—This work was funded by Operating Grants from the Canadian Institutes for Health Research (CIHR) (PJT-162439 to N. B., MOP-126058 to S. B.), from the Canadian Urologic Oncology Group (CUOG) (to L. V. and F. P.) as well as from the Centre de recherche sur le cancer de l'Université Laval (to N. B. and F. P.). L. V. held Pierre-J.-Durand, Jean-François-Bergeron, and Centre de recherche sur le cancer scholarships from Université Laval, as well as Harley Owner's Group-Québec and Louis-Poirier scholarships from the CHU de Québec-Université Laval. C. T. holds a doctoral research scholarship from the Fonds de recherche du Québec. I. B. held a Centre de recherche sur le cancer scholarship from Université Laval. S. B. holds a Canada Research Chair (Tier 2) in Transcriptional Genomics. F. P. holds a senior salary award from the Fonds de Recherche du Québec-Santé (FRQ-S). N.B. was also supported by Leader's Opportunity Funds from the Canada Foundation for Innovation (#30308, #34963) and holds a Canada Research Chair (Tier 2) in Cancer Proteomics.

**Author contributions**—Conceptualization, L. V., F. P., and N. B.; Methodology, L. V., F. L., F.-A. B.-S., C. T., U. D., S. B., F. P., and N. B.; Investigation, L. V., F. L., F.-A. B.-S., C. T., B. N., V. T., I. B., U. D. and N. L.; Writing - original draft, L. V. and N. B.; Writing - review & editing, L. V., F. L., C. T., S. B., F. P., and N. B.; Visualization, L. V., F. L., C. T., and U. D.; Supervision, S. B., F. P., and N. B.; Project Administration, N. B.; Funding Acquisition, F. P. and N. B. All authors read and approved the manuscript.

**Conflict of interest**—The authors declare no competing interests.

**Abbreviations**—The abbreviations used are: AP-MS, affinity purification combined to mass spectrometry; AR, androgen receptor; ARE, androgen response element; DHT, 5 $\alpha$ -dihydrotestosterone; DMAP1, DNA methyltransferase 1 associated protein 1; DNA-PK, DNA-dependent protein kinase; FBS, fetal bovine serum; GFP, green fluorescent protein; GRHL2, grainyhead-like 2; HEK293, human embryonic kidney 293 cells; HSP, heat shock protein; KLF4, Krüppel-like factor 4; KMT2A, lysine methyl transferase 2A; MALDI-TOF, matrix-assisted laser desorption ionization time-of-flight; MED1, MEDIator complex subunit 1; MED12, MEDIator complex subunit 12; NIPBL, NIPBL cohesion loading factor; PCa, prostate cancer; PEI, polyethylenimine; POLH, DNA polymerase eta; PSA, prostate-specific antigen; RIME, rapid immunoprecipitation MS of endogenous proteins; TF, transcription factor.

Received November 6, 2020, and in revised form, February 9, 2021  
Published, MCPRO Papers in Press, February 26, 2021, <https://doi.org/10.1016/j.mcpro.2021.100064>

## REFERENCES

- Siegel, R. L., Miller, K. D., and Jemal, A. (2017) Cancer Statistics, 2017. *CA Cancer J. Clin.* **67**, 7–30
- Bennett, N. C., Gardiner, R. A., Hooper, J. D., Johnson, D. W., and Gobe, G. C. (2010) Molecular cell biology of androgen receptor signalling. *Int. J. Biochem. Cell Biol.* **42**, 813–827
- Cantin, L., Faucher, F., Couture, J. F., de Jesus-Tran, K. P., Legrand, P., Ciobanu, L. C., Frechette, Y., Labrecque, R., Singh, S. M., Labrie, F., and Breton, R. (2007) Structural characterization of the human androgen receptor ligand-binding domain complexed with EM5744, a rationally designed steroidal ligand bearing a bulky chain directed toward helix 12. *J. Biol. Chem.* **282**, 30910–30919
- Helsen, C., Kerkhofs, S., Clinckemalie, L., Spans, L., Laurent, M., Boonen, S., Vanderschueren, D., and Claessens, F. (2012) Structural basis for nuclear hormone receptor DNA binding. *Mol. Cell Endocrinol.* **348**, 411–417
- Ferraldeschi, R., Welts, J., Luo, J., Attard, G., and de Bono, J. S. (2015) Targeting the androgen receptor pathway in castration-resistant prostate cancer: Progresses and prospects. *Oncogene* **34**, 1745–1757
- Mitsiades, N. (2013) A road map to comprehensive androgen receptor axis targeting for castration-resistant prostate cancer. *Cancer Res.* **73**, 4599–4605
- Baron, S., Manin, M., Beaudoin, C., Leotoing, L., Communal, Y., Veysié, G., and Morel, L. (2004) Androgen receptor mediates non-genomic activation of phosphatidylinositol 3-OH kinase in androgen-sensitive epithelial cells. *J. Biol. Chem.* **279**, 14579–14586
- Leung, J. K., and Sadar, M. D. (2017) Non-genomic Actions of the androgen receptor in prostate cancer. *Front Endocrinol. (Lausanne)* **8**, 2
- Ishitani, K., Yoshida, T., Kitagawa, H., Ohta, H., Nozawa, S., and Kato, S. (2003) p54nrb acts as a transcriptional coactivator for activation function 1 of the human androgen receptor. *Biochem. Biophys. Res. Commun.* **306**, 660–665
- Faus, H., Meyer, H. A., Huber, M., Bahr, I., and Haendler, B. (2005) The ubiquitin-specific protease USP10 modulates androgen receptor function. *Mol. Cell Endocrinol.* **245**, 138–146
- Mayeur, G. L., Kung, W. J., Martinez, A., Izumiya, C., Chen, D. J., and Kung, H. J. (2005) Ku is a novel transcriptional recycling coactivator of the androgen receptor in prostate cancer cells. *J. Biol. Chem.* **280**, 10827–10833
- Chen, S. T., Okada, M., Nakato, R., Izumi, K., Bando, M., and Shirahige, K. (2015) The deubiquitinating enzyme USP7 regulates androgen receptor activity by modulating its binding to chromatin. *J. Biol. Chem.* **290**, 21713–21723
- Paltoglou, S., Das, R., Townley, S. L., Hickey, T. E., Tarulli, G. A., Coutinho, I., Fernandes, R., Hanson, A. R., Denis, I., Carroll, J. S., Dehm, S. M., Raj, G. V., Plymate, S. R., Tilley, W. D., and Selth, L. A. (2017) Novel androgen receptor Coregulator GRHL2 Exerts both oncogenic and Antimetastatic functions in prostate cancer. *Cancer Res.* **77**, 3417–3430
- Stelloo, S., Nevedomskaya, E., Kim, Y., Hoekman, L., Bleijerveld, O. B., Mirza, T., Wessels, L. F. A., van Weerden, W. M., Altelar, A. F. M., Bergman, A. M., and Zwart, W. (2018) Endogenous androgen receptor proteomic profiling reveals genomic subcomplex involved in prostate tumorigenesis. *Oncogene* **37**, 313–322
- Hsiao, J. J., Ng, B. H., Smits, M. M., Martinez, H. D., Jasavala, R. J., Hinkson, I. V., Fermin, D., Eng, J. K., Nesvizhskii, A. I., and Wright, M. E. (2015) Research Resource: Androgen receptor activity is regulated through the Mobilization of cell Surface receptor networks. *Mol. Endocrinol.* **29**, 1195–1218
- Hsiao, J. J., Smits, M. M., Ng, B. H., Lee, J., and Wright, M. E. (2016) Discovery proteomics identifies a molecular Link between the Coatomer protein complex I and androgen receptor-dependent transcription. *J. Biol. Chem.* **291**, 18818–18842
- Paliouras, M., Zaman, N., Lumbroso, R., Kapogeorgakis, L., Beitel, L. K., Wang, E., and Trifiro, M. (2011) Dynamic rewiring of the androgen receptor protein interaction network correlates with prostate cancer clinical outcomes. *Integr. Biol. (Camb)* **3**, 1020–1032
- Roux, K. J., Kim, D. I., Raída, M., and Burke, B. (2012) A promiscuous biotin ligase fusion protein identifies proximal and interacting proteins in mammalian cells. *J. Cell Biol.* **196**, 801–810
- Roux, K. J., Kim, D. I., and Burke, B. (2013) BioID: A screen for protein-protein interactions. *Curr. Protoc. Protein Sci.* **74**. Unit 19 23
- Lempiäinen, J. K., Niskanen, E. A., Vuoti, K. M., Lampinen, R. E., Goos, H., Varjosalo, M., and Palvimo, J. J. (2017) Agonist-specific protein interactomes of glucocorticoid and androgen receptor as revealed by proximity mapping. *Mol. Cell Proteomics* **16**, 1462–1474
- Alimirah, F., Chen, J., Xin, H., and Choubey, D. (2006) Androgen receptor auto-regulates its expression by a negative feedback loop through upregulation of IFI16 protein. *FEBS Lett.* **580**, 1659–1664
- Chatr-Aryamontri, A., Oughtred, R., Boucher, L., Rust, J., Chang, C., Kolas, N. K., O'Donnell, L., Oster, S., Theesfeld, C., Sellam, A., Stark, C., Breitkreutz, B. J., Dolinski, K., and Tyers, M. (2017) The BioGRID interaction database: 2017 update. *Nucleic Acids Res.* **45**, D369–D379
- Fahey, M. E., Bennett, M. J., Mahon, C., Jager, S., Pache, L., Kumar, D., Shapiro, A., Rao, K., Chanda, S. K., Craik, C. S., Frankel, A. D., and Krogan, N. J. (2011) GPS-prot: A web-based visualization platform for integrating host-pathogen interaction data. *BMC Bioinformatics* **12**, 298
- Orchard, S., Ammari, M., Aranda, B., Breuza, L., Briganti, L., Broackes-Carter, F., Campbell, N. H., Chavali, G., Chen, C., del-Toro, N., Duesbury, M., Dumousseau, M., Galeota, E., Hinz, U., Iannuccelli, M., et al. (2014) The MIntAct project—IntAct as a common curation platform for 11 molecular interaction databases. *Nucleic Acids Res.* **42**, D358–D363
- Cheng, S., Brzostek, S., Lee, S. R., Hollenberg, A. N., and Balk, S. P. (2002) Inhibition of the dihydrotestosterone-activated androgen receptor by nuclear receptor corepressor. *Mol. Endocrinol.* **16**, 1492–1501
- Wolf, S. S., Patchev, V. K., and Obendorf, M. (2007) A novel variant of the putative demethylase gene, s-JMJD1C, is a coactivator of the AR. *Arch. Biochem. Biophys.* **460**, 56–66

27. van de Wijngaart, D. J., Dubbink, H. J., Molier, M., de Vos, C., Trapman, J., and Jenster, G. (2009) Functional screening of FxxLF-like peptide motifs identifies SMARCD1/BAF60a as an androgen receptor cofactor that modulates TMPRSS2 expression. *Mol. Endocrinol.* **23**, 1776–1786
28. Elvenes, J., Thomassen, E. I., Johnsen, S. S., Kaino, K., Sjøttem, E., and Johansen, T. (2011) Pax6 represses androgen receptor-mediated transactivation by inhibiting recruitment of the coactivator SPBP. *PLoS One* **6**, e24659
29. Neveu, B., Jain, P., Tetu, B., Wu, L., Fradet, Y., and Pouliot, F. (2016) A PCA3 gene-based transcriptional amplification system targeting primary prostate cancer. *Oncotarget* **7**, 1300–1310
30. Beigbeder, A., Velot, L., James, D. A., and Bisson, N. (2016) Sample preparation for mass spectrometry analysis of protein-protein interactions in cancer cell lines and tissues. *Methods Mol. Biol.* **1458**, 339–347
31. Dionne, U., Chartier, F. J. M., Lopez de Los Santos, Y., Lavoie, N., Bernard, D. N., Banerjee, S. L., Otis, F., Jacquet, K., Tremblay, M. G., Jain, M., Bourassa, S., Gish, G. D., Gagne, J. P., Poirier, G. G., Laprise, P., et al. (2018) Direct phosphorylation of SRC Homology 3 Domains by tyrosine kinase receptors Disassembles ligand-induced signaling networks. *Mol. Cell* **70**, 995–1007.e1011
32. Choi, H., Larsen, B., Lin, Z. Y., Breitreutz, A., Mellacheruvu, D., Fermin, D., Qin, Z. S., Tyers, M., Gingras, A. C., and Nesvizhskii, A. I. (2011) Saint: Probabilistic scoring of affinity purification-mass spectrometry data. *Nat. Methods* **8**, 70–73
33. Nesvizhskii, A. I., Keller, A., Kolker, E., and Aebersold, R. (2003) A statistical model for identifying proteins by tandem mass spectrometry. *Anal. Chem.* **75**, 4646–4658
34. Boudaoud, I., Fournier, E., Bagueette, A., Vallee, M., Lamaze, F. C., Droit, A., and Bilodeau, S. (2017) Connected gene Communities Underlie transcriptional changes in Cornelia de Lange Syndrome. *Genetics* **207**, 139–151
35. Fournier, M., Bourriquen, G., Lamaze, F. C., Cote, M. C., Fournier, E., Joly-Beauparlant, C., Caron, V., Gobeil, S., Droit, A., and Bilodeau, S. (2016) FOXA and master transcription factors recruit Mediator and Cohesin to the core transcriptional regulatory circuitry of cancer cells. *Sci. Rep.* **6**, 34962
36. Kagey, M. H., Newman, J. J., Bilodeau, S., Zhan, Y., Orlando, D. A., van Berkum, N. L., Ebmeier, C. C., Goossens, J., Rahl, P. B., Levine, S. S., Taatjes, D. J., Dekker, J., and Young, R. A. (2010) Mediator and cohesin connect gene expression and chromatin architecture. *Nature* **467**, 430–435
37. Bourgey, M., Dali, R., Eveleigh, R., Chen, K. C., Letourneau, L., Fillon, J., Michaud, M., Caron, M., Sandoval, J., Lefebvre, F., Leveque, G., Mercier, E., Bujold, D., Marquis, P., Van, P. T., et al. (2019) GenPipes: An open-source framework for distributed and scalable genomic analyses. *Giga-science* **8**, giz037
38. Bolger, A. M., Lohse, M., and Usadel, B. (2014) Trimmomatic: A flexible trimmer for Illumina sequence data. *Bioinformatics* **30**, 2114–2120
39. Li, H., and Durbin, R. (2009) Fast and accurate short read alignment with Burrows-Wheeler transform. *Bioinformatics* **25**, 1754–1760
40. Zhang, Y., Liu, T., Meyer, C. A., Eeckhoutte, J., Johnson, D. S., Bernstein, B. E., Nusbaum, C., Myers, R. M., Brown, M., Li, W., and Liu, X. S. (2008) Model-based analysis of ChIP-seq (MACS). *Genome Biol.* **9**, R137
41. Ramirez, F., Ryan, D. P., Gruning, B., Bhardwaj, V., Kilpert, F., Richter, A. S., Heyne, S., Dundar, F., and Manke, T. (2016) deepTools2: a next generation web server for deep-sequencing data analysis. *Nucleic Acids Res.* **44**, W160–W165
42. Kent, W. J., Sugnet, C. W., Furey, T. S., Roskin, K. M., Pringle, T. H., Zahler, A. M., and Haussler, D. (2002) The human genome browser at UCSC. *Genome Res.* **12**, 996–1006
43. Klein, K. A., Reiter, R. E., Redula, J., Moradi, H., Zhu, X. L., Brothman, A. R., Lamb, D. J., Marcelli, M., Belldgrun, A., Witte, O. N., and Sawyers, C. L. (1997) Progression of metastatic human prostate cancer to androgen independence in immunodeficient SCID mice. *Nat. Med.* **3**, 402–408
44. van Bokhoven, A., Varella-Garcia, M., Korch, C., Johannes, W. U., Smith, E. E., Miller, H. L., Nordeen, S. K., Miller, G. J., and Lucia, M. S. (2003) Molecular characterization of human prostate carcinoma cell lines. *Prostate* **57**, 205–225
45. Iyer, M., Wu, L., Carey, M., Wang, Y., Smallwood, A., and Gambhir, S. S. (2001) Two-step transcriptional amplification as a method for imaging reporter gene expression using weak promoters. *Proc. Natl. Acad. Sci. U. S. A.* **98**, 14595–14600
46. Wu, L., Matherly, J., Smallwood, A., Adams, J. Y., Billick, E., Belldgrun, A., and Carey, M. (2001) Chimeric PSA enhancers exhibit augmented activity in prostate cancer gene therapy vectors. *Gene Ther.* **8**, 1416–1426
47. Jain, P., Neveu, B., Velot, L., Wu, L., Fradet, Y., and Pouliot, F. (2016) Bioluminescence microscopy as a method to measure Single cell androgen receptor activity Heterogeneous Responses to Antiandrogens. *Sci. Rep.* **6**, 33968
48. Toren, P., Kim, S., Johnson, F., and Zoubeidi, A. (2016) Combined AKT and MEK pathway blockade in pre-clinical models of Enzalutamide-resistant prostate cancer. *PLoS One* **11**, e0152861
49. Teo, G., Liu, G., Zhang, J., Nesvizhskii, A. I., Gingras, A. C., and Choi, H. (2014) SAINTexpress: Improvements and additional features in significance analysis of INteractome software. *J. Proteomics* **100**, 37–43
50. Axlund, S. D., Lambert, J. R., and Nordeen, S. K. (2010) HOXC8 inhibits androgen receptor signaling in human prostate cancer cells by inhibiting SRC-3 recruitment to direct androgen target genes. *Mol. Cancer Res.* **8**, 1643–1655
51. Jaaskelainen, T., Makkonen, H., Visakorpi, T., Kim, J., Roeder, R. G., and Palvimo, J. J. (2012) Histone H2B ubiquitin ligases RNF20 and RNF40 in androgen signaling and prostate cancer cell growth. *Mol. Cell Endocrinol.* **350**, 87–98
52. Vockley, C. M., D'ippolito, A. M., McDowell, I. C., Majoros, W. H., Safi, A., Song, L., Crawford, G. E., and Reddy, T. E. (2016) Direct GR binding Sites potentiate clusters of TF binding across the human genome. *Cell* **166**, 1269–1281.e1219
53. Goo, Y. H., Na, S. Y., Zhang, H., Xu, J., Hong, S., Cheong, J., Lee, S. K., and Lee, J. W. (2004) Interactions between activating signal cointegrator-2 and the tumor suppressor retinoblastoma in androgen receptor transactivation. *J. Biol. Chem.* **279**, 7131–7135
54. Xu, J., Wu, R. C., and O'Malley, B. W. (2009) Normal and cancer-related functions of the p160 steroid receptor co-activator (SRC) family. *Nat. Rev. Cancer* **9**, 615–630
55. Borggrete, T., and Yue, X. (2011) Interactions between subunits of the Mediator complex with gene-specific transcription factors. *Semin. Cell Dev. Biol.* **22**, 759–768
56. Ries, D., and Meisterernst, M. (2011) Control of gene transcription by Mediator in chromatin. *Semin. Cell Dev. Biol.* **22**, 735–740
57. Uhlen, M., Oksvold, P., Fagerberg, L., Lundberg, E., Jonasson, K., Forsberg, M., Zwahlen, M., Kampf, C., Wester, K., Hober, S., Wernerus, H., Bjorling, L., and Ponten, F. (2010) Towards a knowledge-based human protein Atlas. *Nat. Biotechnol.* **28**, 1248–1250
58. Siu, M. K., Suau, F., Chen, W. Y., Tsai, Y. C., Tsai, H. Y., Yeh, H. L., and Liu, Y. N. (2016) KLF4 functions as an activator of the androgen receptor through reciprocal feedback. *Oncogenesis* **5**, e282
59. Wu, Y., Chhipa, R. R., Zhang, H., and Ip, C. (2011) The antiandrogenic effect of finasteride against a mutant androgen receptor. *Cancer Biol. Ther.* **11**, 902–909
60. Evans, P. M., and Liu, C. (2008) Roles of Kruppel-like factor 4 in normal homeostasis, cancer and stem cells. *Acta Biochim. Biophys. Sin (Shanghai)* **40**, 554–564
61. Ghaleb, A. M., and Yang, V. W. (2017) Kruppel-like factor 4 (KLF4): What we currently know. *Gene* **611**, 27–37
62. Polo, J. M., Anderssen, E., Walsh, R. M., Schwarz, B. A., Nefzger, C. M., Lim, S. M., Borkent, M., Apostolou, E., Alaei, S., Cloutier, J., Bar-Nur, O., Cheloufi, S., Stadtfeld, M., Figueroa, M. E., Robinton, D., et al. (2012) A molecular roadmap of reprogramming somatic cells into iPS cells. *Cell* **151**, 1617–1632
63. Akaogi, K., Nakajima, Y., Ito, I., Kawasaki, S., Oie, S. H., Murayama, A., Kimura, K., and Yanagisawa, J. (2009) KLF4 suppresses estrogen-dependent breast cancer growth by inhibiting the transcriptional activity of ERalpha. *Oncogene* **28**, 2894–2902
64. Fei, T., Chen, Y., Xiao, T., Li, W., Cato, L., Zhang, P., Cotter, M. B., Bowden, M., Lis, R. T., Zhao, S. G., Wu, Q., Feng, F. Y., Loda, M., He, H. H., Liu, X. S., et al. (2017) Genome-wide CRISPR screen identifies HNRNPL as a prostate cancer dependency regulating RNA splicing. *Proc. Natl. Acad. Sci. U. S. A.* **114**, E5207–E5215
65. Zhang, L., Zhang, L., Xia, X., He, S., He, H., and Zhao, W. (2016) Kruppel-like factor 4 promotes human osteosarcoma growth and metastasis via regulating CRYAB expression. *Oncotarget* **7**, 30990–31000

66. Hu, W., Jia, Y., Xiao, X., Lv, K., Chen, Y., Wang, L., Luo, X., Liu, T., Li, W., Li, Y., Zhang, C., Yu, Z., Huang, W., Sun, B., and Deng, W. G. (2016) KLF4 downregulates hTERT expression and telomerase activity to inhibit lung carcinoma growth. *Oncotarget* **7**, 52870–52887
67. Wang, J., Place, R. F., Huang, V., Wang, X., Noonan, E. J., Magyar, C. E., Huang, J., and Li, L. C. (2010) Prognostic value and function of KLF4 in prostate cancer: RNAi and vector-mediated overexpression identify KLF4 as an inhibitor of tumor cell growth and migration. *Cancer Res.* **70**, 10182–10191
68. Xu, X., Li, J., Zhu, Y., Xie, B., Wang, X., Wang, S., Xie, H., Yan, H., Ying, Y., Lin, Y., Liu, B., Wang, W., and Zheng, X. (2017) CRISPR-ON-Mediated KLF4 overexpression inhibits the proliferation, migration and invasion of urothelial bladder cancer *in vitro* and *in vivo*. *Oncotarget* **8**, 102078–102087
69. Shie, J. L., Chen, Z. Y., Fu, M., Pestell, R. G., and Tseng, C. C. (2000) Gut-enriched Kruppel-like factor represses cyclin D1 promoter activity through Sp1 motif. *Nucleic Acids Res.* **28**, 2969–2976
70. Vizcaino, J. A., Csordas, A., del-Toro, N., Dianes, J. A., Griss, J., Lavidas, I., Mayer, G., Perez-Riverol, Y., Reisinger, F., Ternent, T., Xu, Q. W., Wang, R., and Hermjakob, H. (2016) 2016 update of the PRIDE database and its related tools. *Nucleic Acids Res.* **44**, D447–D456
71. Edgar, R., Domrachev, M., and Lash, A. E. (2002) Gene expression Omnibus: NCBI gene expression and hybridization array data repository. *Nucleic Acids Res.* **30**, 207–210